Thanks are due to Dr G. Lehmpfuhl for valuable discussions which led the author to the present study.

References

BETHE, H. (1928). *Ann. Phys. (Leipzig)*, **87**, 55-129.
COLELLA, R. (1972). *Acta Cryst.* A**28**, 11-15.
COWLEY, J. M. (1981). *Diffraction Physics.* Amsterdam: North-Holland.
COWLEY, J. M. & MOODIE, A. F. (1957). *Acta Cryst.* **10**, 609-619.
DARWIN, C. G. (1914). *Philos. Mag.* **27**, 315-333, 675-690.
FALK, S. (1984). *Z. Angew. Math. Mech.* **64**, 445-456.
ICHIMIYA, A. (1983). *Jpn. J. Appl. Phys.* **22**, 176-180.
KAMBE, K. (1967). *Z. Naturforsch. Teil A*, **22**, 422-431.
KAMBE, K. & MOLIÈRE, K. (1970). In *Advances in Structure Research by Diffraction Methods*, Vol. 3, edited by R. BRILL & R. MASON, p. 53. Oxford: Pergamon Press.
LAMLA, E. (1938*a*). *Ann. Phys. (Leipzig)*, (5. *Folge*), **32**, 178-189, 225-241.
LAMLA, E. (1938*b*). *J. Rein. Angew. Math.* **179**, 134-142.
LEHMPFUHL, G. & DOWELL, W. C. T. (1986). *Acta Cryst.* A**42**, 569-577.
LEHMPFUHL, G. & MOLIÈRE, K. (1961). *Z. Phys.* **164**, 389-408.
LEHMPFUHL, G. & REISSLAND, A. (1968). *Z. Naturforsch. Teil A*, **23**, 544-549.
LYNCH, D. F. & MOODIE, A. F. (1972). *Surf. Sci.* **32**, 422-438.
MAKSYM, P. A. & BEEBY, J. L. (1981). *Surf. Sci.* **110**, 423-438.
MOON, A. R. (1972). *Z. Naturforsch. Teil A*, **27**, 390-395.
PENDRY, J. B. (1974). *Low Energy Electron Diffraction.* London: Academic Press.
PENDRY, J. B. & GARD, P. (1975). *J. Phys. C*, **8**, 2048-2058.
SOMMERFELD, A. & BETHE, H. (1930). *Handbuch der Physik*, Vol. 24, No. 2. Berlin: Springer. (Available as a paperback, *Heidelberger Taschenbücher*, Vol. 19, 1967).
TOURNARIE, M. (1962). *J. Phys. Soc. Jpn*, **17** Suppl. B-II, 98-100.
ZURMÜHL, R. & FALK, S. (1984). *Matrizen und Ihre Anwendungen*, Vol. 1. Berlin: Springer.

Acta Cryst. (1988). A**44**, 890-897

Interpretation of the Shape of Electron Diffraction Spots from Small Polyhedral Crystals by Means of the Crystal Shape Amplitude

BY W. NEUMANN

Institute of Solid State Physics and Electron Microscopy, Academy of Sciences of the GDR, Weinberg 2, 4020 *Halle/Saale, German Democratic Republic*

J. KOMRSKA

Institute of Scientific Instruments, Czechoslovak Academy of Sciences, Královopolská 147, 612 64 *Brno, Czechoslovakia*

AND H. HOFMEISTER AND J. HEYDENREICH

Institute of Solid State Physics and Electron Microscopy, Academy of Sciences of the GDR, Weinberg 2, 4020 *Halle/Saale, German Democratic Republic*

(*Received* 30 *November* 1987; *accepted* 4 *May* 1988)

Abstract

The influence of the crystal shape on the fine structure of transmission electron diffraction (TED) patterns described by the crystal shape amplitude is discussed. A general algebraic expression for the crystal shape amplitude of any crystal polyhedron is used for computing the intensity distribution of TED reflections. The computer simulation method is applied to the analysis of the fine structure of TED patterns of small gold and palladium crystals having octahedral and tetrahedral habits.

1. Introduction

In electron diffraction of small crystals spots are frequently observed which have distinct fine structure consisting of streaks, satellites or elongations. The shape of any diffraction spot is mainly determined by the shape of the crystal as well as by the presence of crystal defects. The contribution of the crystal shape to the fine structure of the reflections can be described within the framework of the kinematical diffraction theory. The intensity distribution around each reciprocal-lattice point **g** is then given by

$$I_{hkl}(\mathbf{p}) = |F_{hkl}|^2 |S(\mathbf{p})|^2 \qquad (1)$$

where, for the lattice point **g**, F_{hkl} is the structure amplitude and S is the shape amplitude, which is the same around every reflection. In electron diffraction the kinematical approximation usually fails and the exact calculation of the scattered intensities requires a dynamical treatment. A dynamical theory of the

0108-7673/88/060890-08$03.00

electron diffraction from a wedge-shape crystal was given by Kato (1952) and Molière & Niehrs (1954). Detailed theoretical investigations of the fine structure of the spots due to double refraction effects were carried out by Cowley, Goodman & Rees (1957) and further by Molière & Wagenfeld (1958) and Lehmpfuhl & Reissland (1968). [For reviews, see for instance Cowley (1982), Kambe & Molière (1970), Raether (1957)]. It is worth noting, however, that knowledge of the kinematic crystal shape amplitude S is useful and is a good approximation for characterizing the influence of the crystal shape on the intensity distribution of the reflections.

The general concept of the shape amplitude was introduced by von Laue (1936) and later treated by Patterson (1939) and Ewald (1940). Handbooks and textbooks of structure analysis, electron diffraction and electron microscopy present schematic drawings of the shape amplitudes of crystals in the form of needles, spheres, ellipsoids *etc.* Only a few books provide some hints on calculating the shape amplitude in the general case (*e.g.* von Laue, 1948, James, 1967; Hosemann & Bagchi, 1962).

General algebraic expressions were derived by Komrska (1988) which enable numerical evaluation of the shape amplitude of any crystal polyhedron. In this paper the computer simulation of the crystal shape factor of any crystal polyhedron is described by a method using the formulae of Komrska (1988). The computer simulation procedure is applied to the interpretation of the shape of transmission electron diffraction spots from small polyhedral gold crystals and palladium particles. The fine structure of the experimental diffraction spots may be compared with that of 'simulated spots' obtained from the two-dimensional intensity distribution at plane intersections with the corresponding shape amplitudes. The numerical results are presented in the form of so-called crystal shape factor maps representing both central and off-centre cross sections through the shape factor $|S(\mathbf{p})|^2$ by planes perpendicular to the incident electron beam (calculated for the actual crystal orientation).

2. Algebraic formulae for the crystal shape amplitude of a crystal polyhedron

The crystal shape amplitude is the Fourier transform of the crystal shape function (Ewald, 1940). The shape function of the crystal is defined by

$$s(\boldsymbol{\xi}) = \begin{cases} 1 & \text{if } \boldsymbol{\xi} \in V \\ 0 & \text{if } \boldsymbol{\xi} \notin V, \end{cases} \tag{2}$$

V being the volume of the crystal. The shape amplitude is then given by

$$S(\mathbf{p}) = \int_V \exp(-2\pi i \mathbf{p}.\boldsymbol{\xi})\, \mathrm{d}^3\boldsymbol{\xi}. \tag{3}$$

The integral (3) can always be expressed in an algebraic way, if the crystal shape has the form of a polyhedron. Generally, the use of the so-called Abbe transform (*e.g.* Komrska, 1982) enables the volume integral $S(\mathbf{p})$ to be converted into a surface integral, and correspondingly the surface integral to be converted into a line integral along the polygonal boundaries of the faces. The systematic investigations of the various possibilities of expressing the crystal shape factor algebraically for any crystal polyhedron have yielded several formally different formulae, where the shape amplitude is expressed by sums over faces and edges, over faces and vertices, over edges and faces *etc.* (Komrska, 1988). These expressions are not equally suitable for numerical calculations as they involve more or fewer terms, some of which are singular for particular directions of the variable $\mathbf{p}$. The most suitable formula for numerical calculations is that summing the contributions of the crystal faces to the shape amplitude in the following form:

$$S(\mathbf{p}) = -\frac{1}{(2\pi p)^2} \sum_{f=1}^{F} \frac{\mathbf{p}.\mathbf{N}_f}{p^2 - (\mathbf{p}.\mathbf{N}_f)^2} \times \sum_{e=1}^{E_f} L_{fe}\mathbf{p}.(\mathbf{t}_{fe} \times \mathbf{N}_f) \times \frac{\sin(\pi \mathbf{p}.\mathbf{t}_{fe}L_{fe})}{\pi \mathbf{p}.\mathbf{t}_{fe}L_{fe}} \exp(-2\pi i \mathbf{p}.\boldsymbol{\xi}^{(C_{fe})}), \quad \mathbf{p} \neq \pm p\mathbf{N}_f, \tag{4}$$

where F is the number of crystal faces, E_f is the number of edges of the fth crystal face, $\mathbf{N}_f$ is the unit outward normal to the fth face, L_{fe} is the length of the eth edge of the fth face, $\mathbf{t}_{fe}$ is the unit vector in the direction of the eth edge of the fth face, and $\boldsymbol{\xi}^{(C_{fe})}$ is the position vector of the midpoint C_{fe} of the eth edge of the fth face. The vectors $\mathbf{t}_{fe}$ are oriented counterclockwise if viewed in the opposite direction to the outward face normal $\mathbf{N}_f$.

From (4) it becomes evident that if $\mathbf{p}_0$ is perpendicular to a face f_0, *i.e.* if $\mathbf{p}_0 = \pm p_0\mathbf{N}_{f0}$, the corresponding term in the sum is singular, because $p_0^2 - (\mathbf{p}_0.\mathbf{N}_{f0})^2 = 0$. If the crystal possesses F_0 such (mutually parallel) faces, the crystal shape amplitude must be evaluated from the expression

$$S(\mathbf{p}_0) = \frac{i}{2\pi p_0^2} \sum_{f_0=1}^{F_0} \mathbf{p}_0.\mathbf{N}_{f0}P_{f0} \exp(-2\pi i \mathbf{p}_0.\mathbf{N}_{f0}d_{f0}) - \frac{1}{(2\pi p_0)^2} \sum_{f=1}^{F} \frac{\mathbf{p}_0.\mathbf{N}_{f0}}{p^2 - (\mathbf{p}_0.\mathbf{N}_f)^2} \times \sum_{e=1}^{E_f} L_{fe}\mathbf{p}_0.(\mathbf{t}_{fe} \times \mathbf{N}_f) \frac{\sin(\pi \mathbf{p}_0.\mathbf{t}_{fe}L_{fe})}{\pi \mathbf{p}_0.\mathbf{t}_{fe}L_{fe}} \times \exp(-2\pi i \mathbf{p}_0.\boldsymbol{\xi}^{(C_{fe})}), \quad \mathbf{p}_0 = \pm p_0\mathbf{N}_{f0}, \tag{5}$$

where P_{f0} is the area of the face, and d_{f0} is the distance of the f_0th face from the origin.

The shape amplitude of a crystal with a centre of symmetry is a real function and the terms of the sums in (4) and (5) are reduced by a half. For instance, (5) is then given by

$$S(\mathbf{p}_0) = \frac{1}{\pi p_0} \sum_{f_0=1}^{F_0/2} P_{f0} \sin(2\pi p_0 d_{f0}) - \frac{1}{2\pi^2 p_0^2} \sum_{\substack{f=1 \\ f\neq f_0}}^{F/2} \frac{\mathbf{N}_{f0}.\mathbf{N}_f}{1-(\mathbf{N}_{f0}.\mathbf{N}_f)^2} \times \sum_{e=1}^{E_f} L_{fe}\mathbf{N}_{f0}.(\mathbf{t}_{fe}\times\mathbf{N}_f) \frac{\sin(\pi\mathbf{p}_0.\mathbf{t}_{fe}L_{fe})}{\pi\mathbf{p}_0.\mathbf{t}_{fe}L_{fe}} \times \cos(2\pi p_0 \mathbf{N}_{f0}.\boldsymbol{\xi}^{(C_{fe})}), \qquad \mathbf{p}_0 = \pm p_0 \mathbf{N}_{f0}. \tag{6}$$

The main advantage of (4) is that singularities occur only if the reciprocal vector $\mathbf{p}$ is perpendicular to a face and that for these directions (5) is to be applied, the numerical evaluation of which follows the same scheme. The formulae (4) and (5) can be used for the numerical evaluation of the crystal shape amplitude of any crystal polyhedron, if the crystal is specified by the above mentioned quantities.

3. Calculation procedure

In order to interpret the shape of transmission electron diffraction spots of small polyhedral crystals, computer programs were written which enabled the calculation and graphical representation of any desired section and projection through the three-dimensional crystal shape factor $|S(\mathbf{p})|^2$ of any crystal polyhedron. The calculation procedure of $|S(\mathbf{p})|^2 = S(\mathbf{p})S^*(\mathbf{p})$ (the asterisk denotes the complex conjugate expression) is carried out using the algebraic expressions (5) and (6). The procedure applied is advantageous, as the fixed set of quantities describing the geometry of a given polyhedron comprises the input data for all calculations of the shape factor of this polyhedron for any orientation. The orientation relationships are specified by transformation matrices. In the programs the parameter $\mathbf{p}$ is replaced by $\mathbf{x} = 2\pi a\mathbf{p}$, where a is chosen to be a suitable length. For Platonic bodies, for instance, a is the length of the edge of the circumscribed cube (*cf.* Figs. 1, 3, 5, 7). Thus, the calculations are carried out within the dimensionless boundaries of t_i ($i = 1, 2, 3$). The calculated intensity distribution $|S(\mathbf{p})|^2$ of a projection for a given polyhedron can then easily be assigned to any crystal size of this kind of polyhedron. To display the calculated results, a special half-tone overprinting routine is used involving a logarithmic gray scale with 12 gray levels and a special contrast scaling factor, yielding a contrast from white to black for direct comparison with experimental diffraction patterns.

The programs were written in Fortran 77 and the different versions were run on an SM4 computer based on the RSX system as well as on an ICL computer

The algorithm and the programs were tested with the use of the following general properties of the shape amplitude:

(i)

$$\max|S(\mathbf{p})|^2 = S^2(0) = V^2, \tag{7}$$

where V is the volume of the crystal. In the programs the intensity values are normalized by $1/V^2$.

(ii) The shape amplitude $S(\mathbf{p})$ has all the symmetry elements of the shape function $s(\boldsymbol{\xi})$ of the crystal.

(iii)

$$S(\mathbf{p}) = S^*(-\mathbf{p}). \tag{8}$$

For the intensity this becomes

$$|S(\mathbf{p})|^2 = |S(-\mathbf{p})|^2. \tag{9}$$

To illustrate the computational method, the cross sections of the shape factor for a regular pentagonal dodecahedron in $(0\tau 1)$ orientation, *i.e.* parallel to a fivefold axis, are shown in Fig. 1. This example of the calculated fine structure of a diffraction spot caused by the crystal shape might be useful for interpretation of diffraction patterns of small quasi-crystals, where a pentagonal dodecahedral shape is possible. The input data necessary for the calculation of $S(\mathbf{p})$ describing the geometry of the pentagonal dodecahedron are given in Table 1. The central cross section of the shape factor clearly shows the tenfold

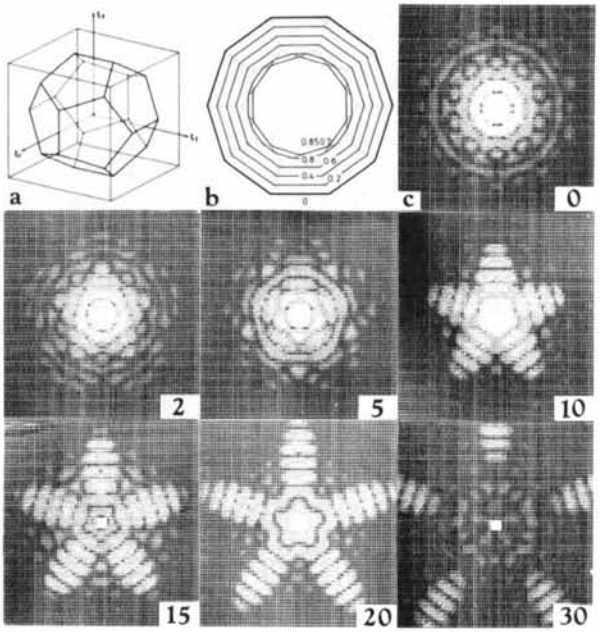

Fig. 1. Crystal shape factor map for a regular pentagonal dodecahedron in $(0\tau 1)$ orientation; (*a*) orientation relationship of pentagonal dodecahedron in circumscribed cube, (*b*) thickness isolines of pentagonal dodecahedron in $(0\tau 1)$ orientation in units of a, (*c*) cross sections of shape factors $|S|^2$; x_1: ±60, x_2: ±60, x_3: 0–30.

Table 1. *Data for calculating the shape amplitude of a pentagonal dodecahedron*

f	N_f	t_{f1}	t_{f2}	t_{f3}	t_{f4}	t_{f5}
1	$A(i+\tau k)$	$\frac{1}{2}(-2j)$	$\frac{1}{2}\left(\tau i-\frac{1}{\tau}j-k\right)$	$\frac{1}{2}\left(i+\tau j-\frac{1}{\tau}k\right)$	$\frac{1}{2}\left(-i+\tau j+\frac{1}{\tau}k\right)$	$\frac{1}{2}\left(-\tau i-\frac{1}{\tau}j+k\right)$
2	$A(-i+\tau k)$	$\frac{1}{2}(2j)$	$\frac{1}{2}\left(-\tau i+\frac{1}{\tau}j-k\right)$	$\frac{1}{2}\left(-i-\tau j-\frac{1}{\tau}k\right)$	$\frac{1}{2}\left(i-\tau j+\frac{1}{\tau}k\right)$	$\frac{1}{2}\left(\tau i+\frac{1}{\tau}j+k\right)$
3	$A(\tau j+k)$	$\frac{1}{2}\left(\tau i+\frac{1}{\tau}j-k\right)$	$\frac{1}{2}\left(-\frac{1}{\tau}i+j-\tau k\right)$	$\frac{1}{2}(-2i)$	$\frac{1}{2}\left(-\frac{1}{\tau}i-j+\tau k\right)$	$\frac{1}{2}\left(\tau i-\frac{1}{\tau}j+k\right)$
4	$A(-\tau j+k)$	$\frac{1}{2}\left(-\tau i-\frac{1}{\tau}j-k\right)$	$\frac{1}{2}\left(\frac{1}{\tau}i-j-\tau k\right)$	$\frac{1}{2}(2i)$	$\frac{1}{2}\left(\frac{1}{\tau}i+j+\tau k\right)$	$\frac{1}{2}\left(-\tau i+\frac{1}{\tau}j+k\right)$
5	$A(\tau i+j)$	$\frac{1}{2}(-2k)$	$\frac{1}{2}\left(-i+\tau j-\frac{1}{\tau}k\right)$	$\frac{1}{2}\left(-\frac{1}{\tau}i+j+\tau k\right)$	$\frac{1}{2}\left(\frac{1}{\tau}i-j+\tau k\right)$	$\frac{1}{2}\left(i-\tau j-\frac{1}{\tau}k\right)$
6	$A(\tau i-j)$	$\frac{1}{2}(2k)$	$\frac{1}{2}\left(-i-\tau j+\frac{1}{\tau}k\right)$	$\frac{1}{2}\left(-\frac{1}{\tau}i-j-\tau k\right)$	$\frac{1}{2}\left(\frac{1}{\tau}i+j-\tau k\right)$	$\frac{1}{2}\left(i+\tau j+\frac{1}{\tau}k\right)$

$A=(\tau^2+1)^{-1/2}$; $L=a/\tau^2=a(2-\tau)$; $V=a^3(\frac{3}{2}\tau-2)$; $P_f=5(4-\tau^2)^{-1/2}a^2/4\tau^3\simeq 0{\cdot}2510\,a^2$;
$d_f=a/[2-\sqrt{5}(\sqrt{5}-1)]^{1/2}$; $\tau=(1+\sqrt{5})/2$

f	$\xi^{(C_{f1})}$	$\xi^{(C_{f2})}$	$\xi^{(C_{f3})}$	$\xi^{(C_{f4})}$	$\xi^{(C_{f5})}$
1	$\frac{a}{4}(2k)$	$\frac{a}{4}\left(\frac{1}{\tau}i-j+k\right)$	$\frac{a}{4}\left(\tau i-\frac{1}{\tau}j+k\right)$	$\frac{a}{4}\left(\tau i+\frac{1}{\tau}j+k\right)$	$\frac{a}{4}\left(\frac{1}{\tau}i+j+\tau k\right)$
2	$\frac{a}{4}(2k)$	$\frac{a}{4}\left(-\frac{1}{\tau}i+j+\tau k\right)$	$\frac{a}{4}\left(-\tau i+\frac{1}{\tau}j+k\right)$	$\frac{a}{4}\left(-\tau i-\frac{1}{\tau}j+k\right)$	$\frac{a}{4}\left(-\frac{1}{\tau}i-j+\tau k\right)$
3	$\frac{a}{4}\left(\frac{1}{\tau}i+j+\tau k\right)$	$\frac{a}{4}\left(i+\tau j+\frac{1}{\tau}k\right)$	$\frac{a}{4}(2j)$	$\frac{a}{4}\left(-i+\tau j+\frac{1}{\tau}k\right)$	$\frac{a}{4}\left(-\frac{1}{\tau}i+j+\tau k\right)$
4	$\frac{a}{4}\left(-\frac{1}{\tau}i-j+\tau k\right)$	$\frac{a}{4}\left(-i-\tau j+\frac{1}{\tau}k\right)$	$\frac{a}{4}(-2j)$	$\frac{a}{4}\left(i-\tau j+\frac{1}{\tau}k\right)$	$\frac{a}{4}\left(\frac{1}{\tau}i-j+\tau k\right)$
5	$\frac{a}{4}(2i)$	$\frac{a}{4}\left(\tau i+\frac{1}{\tau}j-k\right)$	$\frac{a}{4}\left(i+\tau j-\frac{1}{\tau}k\right)$	$\frac{a}{4}\left(i+\tau j+\frac{1}{\tau}k\right)$	$\frac{a}{4}\left(\tau i+\frac{1}{\tau}j+k\right)$
6	$\frac{a}{4}(2i)$	$\frac{a}{4}\left(\tau i-\frac{1}{\tau}j+k\right)$	$\frac{a}{4}\left(i-\tau j+\frac{1}{\tau}k\right)$	$\frac{a}{4}\left(i-\tau j+\frac{1}{\tau}k\right)$	$\frac{a}{4}\left(\tau i-\frac{1}{\tau}j-k\right)$

Table 2. *Correspondence between the x_3, ξ_3 parameters, and the tilt angle ε*

Crystal	$L_{oct}\sim 650$ Å $a\sim 920$ Å		$L_{oct}\sim 700$ Å $a\sim 990$ Å		$L_{tet}\sim 750$ Å $a\sim 530$ Å	
$\lvert x_3\rvert$	$\lvert\zeta_3\rvert\simeq\lvert p_3\rvert$(Å^{-1})	$\lvert\varepsilon\rvert$(°)	$\lvert\zeta_3\rvert\simeq\lvert p_3\rvert$(Å^{-1})	$\lvert\varepsilon\rvert$(°)	$\lvert\zeta_3\rvert\simeq\lvert p_3\rvert$(Å^{-1})	$\lvert\varepsilon\rvert$(°)
2	$3{\cdot}46\times10^{-4}$	0·04	$3{\cdot}22\times10^{-4}$	0·02	$6{\cdot}01\times10^{-4}$	0·04
5	$8{\cdot}65\times10^{-4}$	0·1	$8{\cdot}04\times10^{-4}$	0·06	$1{\cdot}50\times10^{-3}$	0·1
10	$1{\cdot}73\times10^{-3}$	0·2	$1{\cdot}61\times10^{-3}$	0·1	$3{\cdot}00\times10^{-3}$	0·2
15	$2{\cdot}60\times10^{-3}$	0·3	$2{\cdot}41\times10^{-3}$	0·2	$4{\cdot}50\times10^{-3}$	0·3
20	$3{\cdot}46\times10^{-3}$	0·4	$3{\cdot}22\times10^{-3}$	0·3	$6{\cdot}01\times10^{-3}$	0·5
30	$5{\cdot}19\times10^{-3}$	0·6	$4{\cdot}82\times10^{-3}$	0·4	$9{\cdot}01\times10^{-3}$	0·7
Bragg condition	**g**[200] $\lvert\zeta_g\rvert=4{\cdot}47\times10^{-3}$	0·52	**g**[220] $\lvert\zeta_g\rvert=8{\cdot}93\times10^{-3}$	0·74	**g**[220] $\lvert\zeta_g\rvert=1{\cdot}02\times10^{-2}$	0·78

symmetry corresponding to the fivefold axis of $s(\xi)$. The off-centre cross sections obviously exhibit the loss of the centrosymmetry which leads to the fivefold symmetrical cross section. The different x_3 values can be assigned to the corresponding ζ_3 components of the actual deviation parameter ζ of a diffraction spot from the Ewald sphere for any given size of the pentagonal dodecahedron.

4. Applications

The structure and habit of small gold crystals ($a_0=4{\cdot}07$ Å) and of palladium particles ($a_0=3{\cdot}809$ Å) were investigated by various transmission electron microscope imaging techniques and by transmission electron diffraction (Hofmeister, Haefke & Krohn, 1982). The metal particles grown by vapour deposition onto ionic crystal substrates (Au/AgBr; Pd/KI) exhibit a clearly distinguishable polyhedral shape of mainly octahedral habit. For palladium particles a tetrahedral shape was observed, too. By illuminating the specimens by a highly collimated electron beam very sharp diffraction patterns of the particles in various orientations could be obtained. The shape of the spots is characteristic of the particle orientation. The fine structure of the diffraction spots was compared with calculated maps presenting both central and off-centre cross sections through the shape factor

$|S(\mathbf{p})|^2$ by planes perpendicular to the electron beam. The correspondence between the x_3 value of the shape factor maps and the ζ_3 values for the actual crystal size as well as the related tilt angles $|\varepsilon| = |\boldsymbol{\zeta}|/\mathbf{g}$ are given in Table 2. The selected area electron diffraction pattern (SAED) of the octahedral gold particle in (001) orientation is given in Fig. 2(*a*). The details of the fine structure of two different 200 reflections are clearly displayed in Figs. 2(*b*) and 2(*c*), respectively. The computer-simulated shape factor map of an octahedron in (001) orientation (Fig. 3) demonstrates the change of the intensity distribution related to the various off-centre sections. The intensity distribution of the reflections of the diffraction pattern exhibits a slight deviation from the exact (001) orientation. The main features of the fine structure of the 200 reflections can be correlated with the calculated cross section images ranging from $x_3 = 15$ to $x_3 = 30$. The actual size of the gold crystal determined from a TEM bright-field image was 650 Å. For this size the x_3 values from 15 to 30 correspond to a misorientation of 0·1–0·2° from the exact (001) orientation.

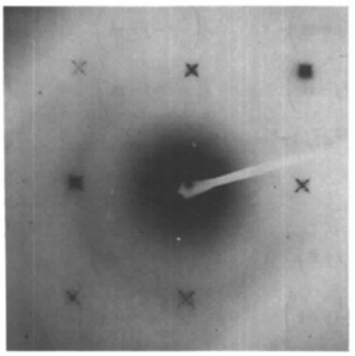

(*a*)

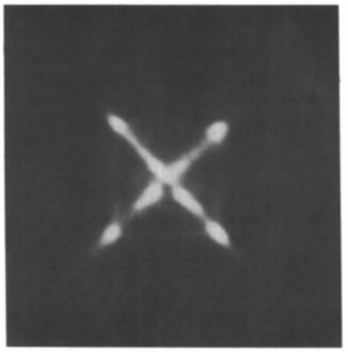

(*b*)

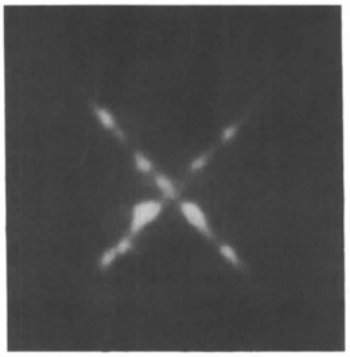

(*c*)

Fig. 2. Electron diffraction of an octahedral gold crystal in (001) orientation; (*a*) SAED pattern, (*b*), (*c*) fine structure of 200 reflections.

The SAED pattern as well as the fine structure of two different 220 reflections of an octahedral gold crystal ($L_{oct} = 700$ Å) in (111) orientation are shown in Fig. 4. The corresponding crystal shape factor map for this orientation is given in Fig. 5. If the experimental parameters [crystal size, slight tilt away from the exact (111) orientation] are taken into consideration, the fine structure of the 220 reflections should be correlated with simulated cross sections ranging from $x_3 = 15$ to $x_3 = 30$, which corresponds to a tilt of 0·2–0·5° away from the symmetrical excitation ($|\zeta_{220}| = 8{\cdot}93 \times 10^{-3}$ Å^{-1}).

An example of the fine structure of 220 reflections of the small palladium crystal of tetrahedral shape in (111) orientation is given in Fig. 6. The comparison of the fine structure of the two 220 reflections with the calculated cross sections of the shape factor map (Fig. 7) reveals a relatively good correlation with the

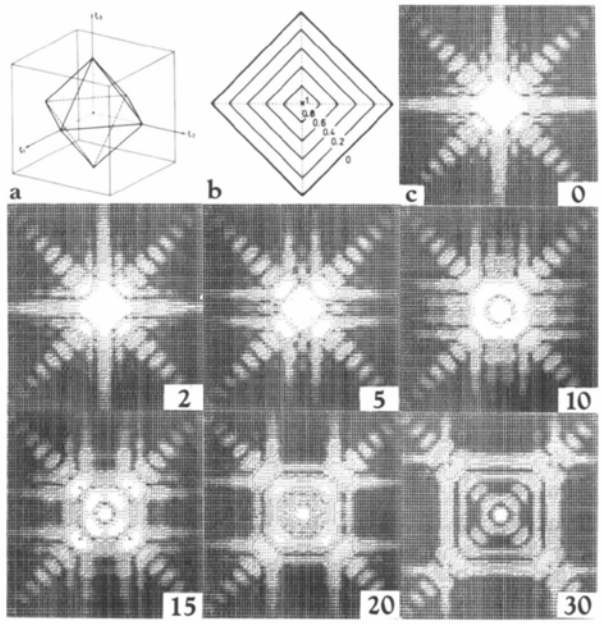

Fig. 3. Crystal shape factor map for an octahedron in (001) orientation; (*a*) orientation relationship of octahedron in circumscribed cube, (*b*) thickness isolines of octahedron in (001) orientation given in units of *a*, (*c*) cross sections of shape factors $|S|^2$; x_1: ±60, x_2: ±60, x_3: 0–30.

sections ranging from $x_3 = 10$ to $x_3 = 20$. This range corresponds to a deviation of 0·1–0·4° from the exact Bragg condition.

5. Discussion

Our results indicate that the method of computer simulation of the crystal shape factor can be used, in principle, for the interpretation of the shape and symmetry of diffraction spots of small polyhedral crystals. The maximum thickness t of the gold and palladium crystals investigated (particle I Au: $t_{(001)} \sim 920$, $t_{(111)} \sim 530$ Å; particle II Au: $t_{111} \sim 570$ Å; Pd: $t_{111} \sim 610$ Å) lies in the dynamical range. The dynamical scattering leads to alterations in the intensity of the reflections and in the intensity distribution of the fine structure of a single reflection as can be clearly seen in the experimental electron diffraction patterns. However, the fine structure of all diffraction spots considered exhibits symmetry relationships which are consistent with the symmetry of the calculated cross sections of the shape factor maps. Thus, the influence of the 'dynamic shape transform' (Cowley, Goodman & Rees, 1957) is not very obvious in the experiments described. We therefore reach the conclusion that the method described can be applied generally to the interpretation of the main features of the fine structure of electron diffraction spots from small polyhedral crystals as a good approximation. In describing the possibilities of obtaining a better correlation between the observed intensity distribution of the the diffraction spots and the simulated ones, the following aspects have to be taken into consideration:

The small crystals investigated very often exhibit additional morphological features (*e.g.* facets) creating additional streaks and satellites as a mixture of the polyhedral faces and the surface topography. The change of the fine structure of the diffraction spots of an octahedral crystal as a function of the degree of truncations at the vertices of the octahedron was

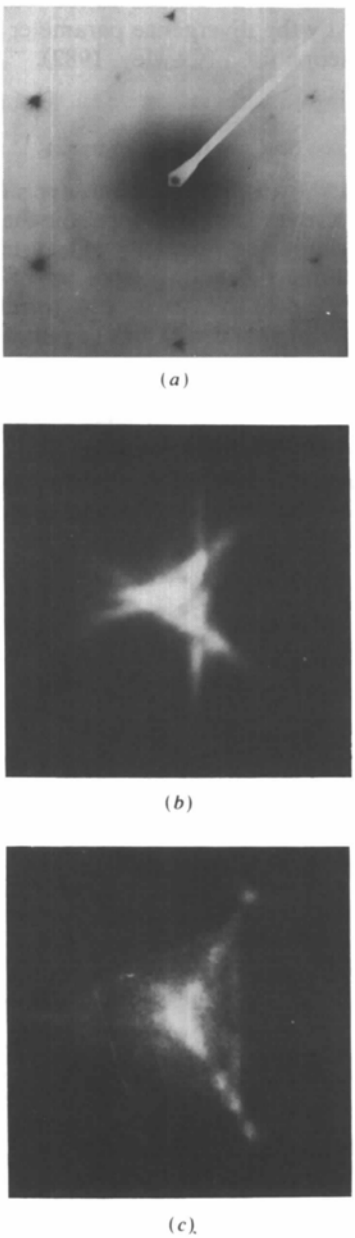

(*a*)

(*b*)

(*c*)

Fig. 4. Electron diffraction of an octahedral gold crystal in (111) orientation; (*a*) SAED pattern, (*b*), (*c*) fine structure of 220 reflections.

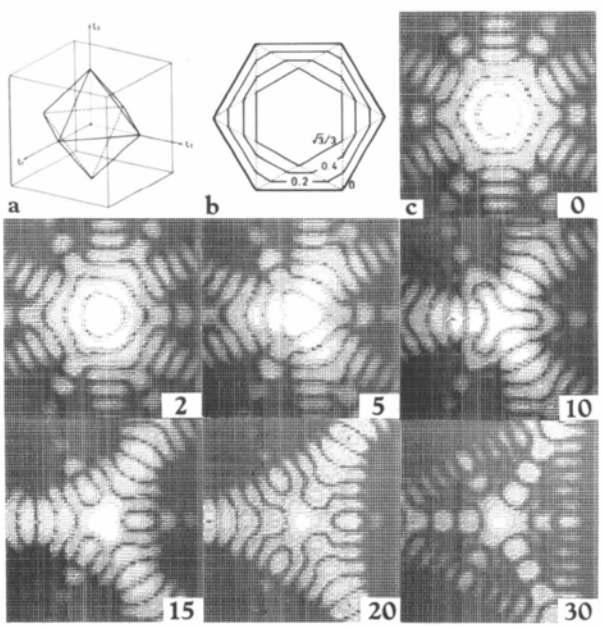

Fig. 5. Crystal shape factor map for an octahedron in (111) orientation; (*a*) orientation relationship of octahedron in circumscribed cube, (*b*) thickness isolines of octahedron in (111) orientation given in units of a, (*c*) cross sections of shape factors $|S|^2$; x_1: ±60, x_2: ±60, x_3: 0–30.

investigated by Hofmeister, Neumann & Komrska (1986). The influence of the surface morphology (terraces, facets, *etc.*) can also be included in the simulation method.

With regard to the experimental conditions, the observed intensity distribution of the diffraction patterns is strongly influenced by the finite source size (beam divergence) and by a limited resolution of photographic plates. In the computer programs a special contrast parameter controls the sensitivity of the contrast (optical density range) which can be adapted to the experimental parameters. The computer simulation experiments were carried out with such a contrast scaling parameter which reveals the details of the function $|S(\mathbf{p})|^2$ with sufficient resolution. The photographically recorded diffraction spots represent a much more limited range of intensities where the fine structure of the reflections is not displayed with sufficiently different gray shadows.

The finite source size, *i.e.* the beam divergence, causes a spread of the intensity. To take this effect into consideration we should have to convolute the crystal shape factor with the so-called source function determined by the divergence parameter of the electron microscope used (Cowley, 1982).

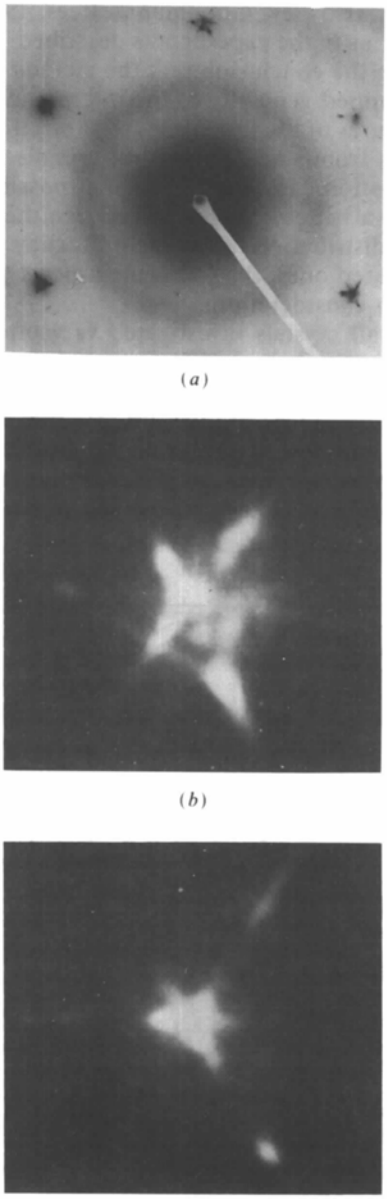

(*a*)

(*b*)

(*c*)

Fig. 6. Electron diffraction of a tetrahedral palladium crystal in (111) orientation; (*a*) SAED pattern, (*b*), (*c*) fine structure of 220 reflections.

6. Concluding remarks

It has been shown that the computer simulation of the crystal shape factor is helpful for the interpretation of the shape and symmetry of transmission electron diffraction reflections from small polyhedral crystals. A series of diffraction patterns taken at well defined experimental conditions (*e.g.* highly coherent illumination, adjusted tilt experiments, specified film parameters) will provide the necessary intensity data for a qualitative analysis. Using the image matching technique (experiments–computer simulated TED patterns) one can gain information on the structure and shape of small crystals. The computer simulation

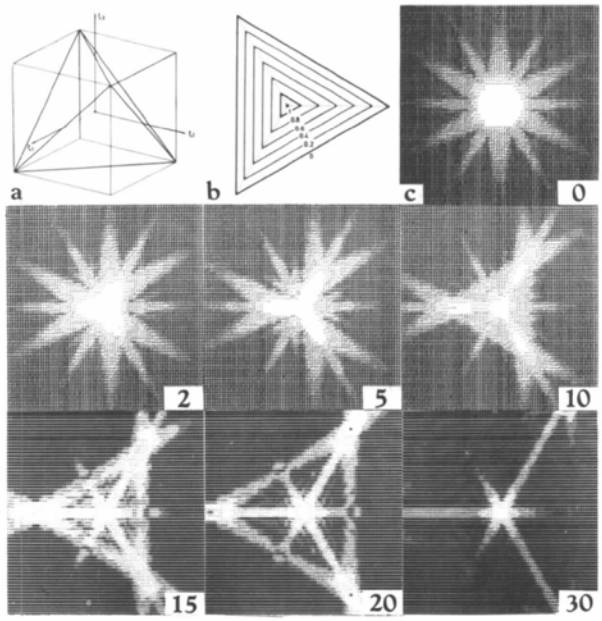

Fig. 7. Crystal shape factor map for a tetrahedron in (111) orientation; (*a*) orientation relationship of tetrahedron in circumscribed cube, (*b*) thickness isolines of tetrahedron in (111) orientation given in units of *a*, (*c*) cross sections of shape factors $|S|^2$; x_1: ±60, x_2: ±60, x_3: 0–30.

of the crystal shape factor seems also to be appropriate for the analysis of the fine structure of the diffraction spots of multiply twinned particles. Calculations to explain the results of experimental investigations of multiply twinned gold particles (Hofmeister, 1984) are in preparation.

The authors are grateful to Professor A. Delong and Professor V. Schmidt for continuing interest and suggestions promoting this cooperative work. They are especially indebted to Dr R. Hillebrand for permission to use his overprinting subroutine as part of our computer programs. Thanks are also due to Mrs Kolaříková for her assistance in preparing the typescript.

References

COWLEY, J. M. (1982). *Diffraction Physics*, 2nd ed., pp. 112, 187-191, 201-218. Amsterdam: North-Holland.

COWLEY, J. M., GOODMAN, P. & REES, A. L. G. (1957). *Acta Cryst.* **10**, 19-25.

EWALD, P. P. (1940). *Proc. Phys. Soc. London*, **52**, 167-174.

HOFMEISTER, H. (1984). *Thin Solid Films*, **116**, 151-162.

HOFMEISTER, H., HAEFKE, H. & KROHN, M. (1982). *J. Cryst. Growth*, **58**, 507-516.

HOFMEISTER, H., NEUMANN, W. & KOMRSKA, J. (1986). Tenth Eur. Crystallogr. Meet., Wrocław, Poland. Abstracts, pp. 371-372.

HOSEMANN, R. & BAGCHI, S. N. (1962). *Direct Analysis of Diffraction by Matter*, pp. 96-109. Amsterdam: North-Holland.

JAMES, R. W. (1967). *The Optical Principles of the Diffraction of X-rays*, p. 55. London: Bell.

KAMBE, K. & MOLIÈRE, K. (1970). *Dynamical Theory of Electron Diffraction.* In *Advances in Structure Research by Diffraction Methods*, edited by R. BRILL & R. MASON, Vol. 3, pp. 53-100. Braunschweig: Vieweg.

KATO, N. (1952). *J. Phys. Soc. Jpn*, **7**, 397-406.

KOMRSKA, J. (1982). *J. Opt. Soc. Am.* **72**, 1382-1384; **73**, 864.

KOMRSKA, J. (1988). *Czech. J. Phys. B.* Submitted.

LAUE, M. VON (1936). *Ann. Phys. (Leipzig)* (5. *Folge*), **26**, 55-68.

LAUE, M. VON (1948). *Materiewellen und ihre Interferenzen*, 2nd ed., pp. 168-186. Leipzig: Akademische Verlagsgesellschaft Geest & Partig K-G.

LEHMPFUHL, G. & REISSLAND, A. (1968). *Z. Naturforsch. Teil A*, **23**, 544-549.

MOLIÈRE, K. & NIEHRS, H. (1954). *Z. Phys.* **137**, 445-462.

MOLIÈRE, K. & WAGENFELD, H. (1958). *Z. Kristallogr.* **110**, 175-196.

PATTERSON, A. L. (1939). *Phys. Rev.* **56**, 972-977.

RAETHER, H. (1957). *Elektroneninterferenzen.* In *Handbuch der Physik*, edited by S. FLÜGGE, Bd XXXII, *Strukturforschung*, pp. 443-551. Berlin: Springer-Verlag.

Acta Cryst. (1988). A**44**, 897-904

Stacking Disorder in a Stage-4 $FeCl_3$–Graphite Intercalation Compound

BY S. HASHIMOTO, K. FORSTER AND S. C. MOSS

Physics Department, University of Houston, Houston, TX 77004, *USA*

(*Received* 1 *December* 1987; *accepted* 10 *May* 1988)

Abstract

X-ray scattering measurements have been made *in situ* on highly oriented pyrolytic graphite intercalated with $FeCl_3$ to stage 4 in a sealed glass tube at 620 K. It has been found that the $FeCl_3$ is in a two-dimensional liquid state at this temperature and that the stacking of the sets of ordered graphite layers (*ABAB*) that bound the intercalant is nearly random. Through a novel modeling of L scans for $10.L$, $11.L$, $20.L$, $21.L$, $30.L$ and $22.L$, a good fit has been achieved by using 60% of a preferred (*A*-*A*) stacking of sets with a broad lateral distribution about the ordered position. The remaining 40% of the sets are stacked with complete translational randomness, without regard to the normal graphite crystallography. This sliding randomness remains compatible with Daumas-Herold domain formation.

I. Introduction

A variety of structural behavior appears in graphite intercalation compounds (GIC's) depending critically on the molecular nature of the species intercalated within the graphite host. With the acceptor compounds, there are often rather complex sequences of ordering reactions involving transitions from liquid to incommensurate solid to commensurate solid (Dresselhaus & Dresselhaus, 1981; Solin, 1982; Moret, 1986). In the case of $FeCl_3$, beginning with the early electron diffraction study by Cowley & Ibers (1956), there has been extensive structural characterization, mainly by Metz and co-workers (Hohlwein & Metz, 1974; Metz & Schulze, 1975; Metz & Hohlwein, 1975). A major feature of these photographic studies, common to all the GIC's, has been the occurrence of well defined stages in which, for

0108-7673/88/060897-08$03.00